

KEK–TH–1458
 LTH 913
 IPPP/11/18
 DCPT/11/36
 TU–883
 15 June 2011

$(g - 2)_\mu$ and $\alpha(M_Z^2)$ re-evaluated using new precise data

KAORU HAGIWARA^a, RUOFAN LIAO^b, ALAN D. MARTIN^c, DAISUKE NOMURA^d
 and THOMAS TEUBNER^b

^a *KEK Theory Center and Sokendai, Tsukuba, 305-0801 Japan*

^b *Department of Mathematical Sciences,
 University of Liverpool, Liverpool L69 3BX, U.K.*

^c *Department of Physics and Institute for Particle Physics Phenomenology,
 University of Durham, Durham DH1 3LE, U.K.*

^d *Department of Physics, Tohoku University, Sendai 980-8578, Japan*

Abstract

We update our Standard Model predictions for $g - 2$ of the muon and for the hadronic contributions to the running of the QED coupling, $\Delta\alpha_{\text{had}}^{(5)}(M_Z^2)$. Particular emphasis is put on recent changes in the hadronic contributions from new data in the 2π channel and from the energy region just below 2 GeV. In particular, for the $e^+e^- \rightarrow \pi^+\pi^-$ contribution we include the recent ‘radiative return’ data from KLOE and BaBar. We also include the recent BaBar data on other exclusive channels. We make a detailed study of the effect of replacing the measurements of the inclusive cross section, $\sigma(e^+e^- \rightarrow \text{hadrons})$, by the sum of the exclusive channels in the energy interval $1.43 < \sqrt{s} < 2$ GeV, which includes a QCD sum-rule analysis of this energy region. Our favoured prediction for the muon anomalous magnetic moment is $(g-2)/2 = (11\,659\,182.8 \pm 4.9) \cdot 10^{-10}$ which is 3.3σ below the present world-average measurement. We compare our $g - 2$ value with other recent calculations. Our prediction for the QED coupling, obtained via $\Delta\alpha_{\text{had}}^{(5)}(M_Z^2) = (276.26 \pm 1.38) \cdot 10^{-4}$, is $\alpha(M_Z^2)^{-1} = 128.944 \pm 0.019$.

1 Introduction

The anomalous magnetic moment of the muon, $a_\mu = (g - 2)_\mu/2$, provides one of the strongest tests of the Standard Model (SM). The discrepancy between the formidable measurement from BNL [1] and the theoretical prediction of a_μ is currently one of the few, if not the only sign for physics beyond the SM (apart from neutrino masses). At present, the discrepancy stands at about three standard deviations, with comparable accuracy between experiment and theory. Clearly, further progress is needed to scrutinize, and possibly firmly establish, this discrepancy. On the theoretical side, this will require first and foremost the improvement of the hadronic contributions which dominate the uncertainty of the SM prediction. The hadronic contributions are usually divided into the leading-order (LO) and higher-order (HO) vacuum polarisation (VP) contributions, and the so-called light-by-light scattering contributions, which are also subleading in terms of the power counting in the coupling α :

$$a_\mu^{\text{had}} = a_\mu^{\text{had, LO VP}} + a_\mu^{\text{had, HO VP}} + a_\mu^{\text{had, l-by-l}}. \quad (1)$$

None of these contributions can be calculated reliably using perturbative QCD (pQCD), as virtual photons with low q^2 dominate the loop integrals. For the light-by-light contributions one relies on model-calculations. A brief discussion of the status of these will be given below when compiling our complete SM prediction of $g - 2$. Fortunately, the situation is better under control for the VP contributions which are large compared to the light-by-light corrections; they can be predicted via dispersion integrals and the experimentally measured hadronic cross section, $\sigma(e^+e^- \rightarrow \gamma^* \rightarrow \text{hadrons})$. For $a_\mu^{\text{had, LO VP}}$ the relation reads

$$a_\mu^{\text{had, LO VP}} = \frac{1}{4\pi^3} \int_{m_\pi^2}^{\infty} ds \sigma_{\text{had}}^0(s) K(s), \quad (2)$$

where $\sigma_{\text{had}}^0(s)$ is the undressed total hadronic cross section (i.e. excluding VP corrections), and K is a well known kernel function given, e.g., by Eq. (45) in the first reference of [2]. (Note that the normalisation of K used here differs by the factor $m_\mu^2/(3s)$.) At present a precision of about 1% is required for the hadronic contributions. So it is mandatory to combine, in the most reliable and consistent way, the best available measurements from many experiments. Recently, several new measurements have become available, both from ‘direct scan’ experiments (like CMD-2 and SND at Novosibirsk’s VEPP, and BES at Beijing’s BEPC), and also the radiative return data obtained in the recent analyses from KLOE [3, 4] and BaBar [5].

The main purpose of this work is to update our calculations [2, 6] of the hadronic vacuum polarisation (HVP) contributions to $g - 2$ and $\Delta\alpha(M_Z^2)$. In section 2 we discuss recent changes in the HVP contributions to $g - 2$, detailing in subsection 2.1 the progress due to radiative return analyses in the most important 2π channel. In subsection 2.2 we study improvements in the important energy region below 2 GeV. In section 3 our updated complete SM prediction of $g - 2$ is given and compared to the BNL measurement and other recent calculations of $g - 2$. Our updated evaluation of $\Delta\alpha(M_Z^2)$ is discussed in section 4. Section 5 contains our conclusions and outlook.

2 Hadronic Vacuum Polarisation Contributions

Since our last major update [6] there have been significant additions to the data input for σ_{had}^0 . Most important, new precise data in the 2π channel have become available, based on radiative return¹ analyses from KLOE [3, 4] and BaBar [5]. These data constitute a crucial check of the previous measurements performed via the traditional method of energy scan by adjusting the e^+, e^- beams, and their impact will be discussed in some detail below. Also, many new data sets in subleading channels have been published, especially in the region just below 2 GeV where BaBar has measured many hadronic cross sections using radiative return. In the following we will concentrate on these two energy regions, before presenting our new results for $a_\mu^{\text{had, LO VP}}$ and $a_\mu^{\text{had, HO VP}}$.

2.1 Data combination and inclusion of data from radiative return experiments in the 2π channel

In the dispersion integral (2), the kernel function K has the form $K = m_\mu^2/(3s) \cdot (0.4 \dots 1)$, where the term in brackets stands for a function which increases monotonically from 0.4 to 1. This results in a strong weighting towards low energies and hence the dominance of the $\rho \rightarrow 2\pi$ channel, which makes up more than 70% of a_μ^{had} . In recent years this channel has been measured very precisely via the direct scan method (adjusting the e^+, e^- beam energy) by the CMD-2 and SND experiments at Novosibirsk, see e.g. [8] for a brief review of their results. From 2005 onwards, analyses based on the method of radiative return have also become available. The first analysis of this kind for the 2π channel was published by KLOE [9], and their 2π distribution agreed fairly well with the measurements from CMD-2 and SND, although there were some shape-differences compared to the CMD-2 and SND data.

In [6] we had already taken into account these KLOE data which were published in 2005. However, the slight difference in shape had made it difficult to combine the KLOE data with all the other 2π data sets on a bin-to-bin basis, and we had hence combined the KLOE data only *after* the dispersion integration, see the detailed discussion in [6]. However, a combination of all data sets in one spectral function and on the same footing, i.e. *before integration*, is clearly preferable, as possible inconsistencies between different data sets will lead to a well-defined error estimate in the data compilation and hence in a_μ^{had} . Therefore, in the current analysis, we have included all data sets in the same way, by performing a χ_{min}^2 fit similar to our original procedure, as described in detail in [2]. This includes the new $2\pi(\gamma)$ data from the radiative return analyses of KLOE [3, 4]² and BaBar [5].

For the data sets from BaBar and KLOE full covariance matrices for statistical and systematic errors are available. To take these into account consistently, our original χ^2 function has to be modified to include additional contributions from non-diagonal elements of the covariance

¹For a review of this method, further references and recent results see [7].

²Note that the KLOE08 data [3] supersede their earlier analysis from 2005 [9], which is therefore discarded in our new compilation.

matrices for the single data sets. The function now reads

$$\begin{aligned} \chi^2(R_m, f_k) = & \sum_{k=1}^{N_{\text{exp}}} \left(\frac{1 - f_k}{df_k} \right)^2 + \\ & \left\{ \sum_{m=1}^{N_{\text{clu}}} \sum_{i=1}^{N(k,m)} \left(\frac{R_i^{(k,m)} - f_k R_m}{dR_i^{(k,m)}} \right)^2 \right\}_{\text{w/out cov. mat.}} + \\ & \sum_{m,n=1}^{N_{\text{clu}}} \sum_{i=1}^{N(k,m)} \sum_{j=1}^{N(k,n)} \left(R_i^{(k,m)} - f_k R_m \right) C^{-1}(m_i, n_j) \left(R_j^{(k,n)} - f_k R_n \right), \quad (3) \end{aligned}$$

where the notation of [2] has been adopted. The final term of the χ^2 function (3) allows the inclusion of the full covariance matrices as given for individual data sets; here C^{-1} denotes the inverse of the matrix C which is the sum of the statistical and systematic covariance matrices of the data set contributing to the specific term in the triple sum.³ The subscript ‘w/out cov. mat.’ in the penultimate term indicates that contributions taken into account via a full covariance matrix are excluded to avoid double counting. For example, BaBar gives experimental uncertainties in the form of a covariance matrix which contains “non-diagonal statistical errors”. In such cases, we take the statistical and systematic contributions to the χ^2 function into account in the third term (and the common systematic error in the first term), but do not include them in the second term. For those experiments whose experimental uncertainties can be considered as an overall systematic and (diagonal) statistical errors, we take them into account in the first and second term, but not in the third term. As in our previous works, this non-linear χ^2 function is minimised numerically, returning the fitted ‘cluster’ (energy bin) mean values R_m and renormalisation factors f_k , in addition to the full covariance matrix of the fit which is used for our error estimate in the prediction of a_μ^{had} and $\Delta\alpha$.⁴ In [2, 6] we had applied error inflation by the global $\sqrt{\chi_{\text{min}}^2/\text{d.o.f.}}$ if bigger than one, indicating that the data are not compatible within errors. However, this may be considered a crude approximation, especially in the case of a_μ where the weighting in the dispersion integral is far from flat. Therefore we have improved the error estimate by employing local χ^2 inflation. This is achieved by calculating, for the preferred binning (judged by the global $\chi_{\text{min}}^2/\text{d.o.f.}$ in the respective channel), a *local χ^2 in each cluster*. This is then used to inflate the error locally when calculating the error by use of the full covariance matrix. The errors obtained in this way vary slightly from the ones based on global χ^2 inflation and are smaller in most channels. This is indicated in Table 1, where, for the most important channels, the global $\chi_{\text{min}}^2/\text{d.o.f.}$ is displayed together with the errors based on global and local error inflation and their difference. For the numbers used in this analysis, we will use local inflation whenever applicable.

³Note that all the common systematic errors are already taken into account via df_k in the first term of the χ^2 function and therefore subtracted from the matrices C .

⁴We do not attempt to estimate correlations between different experiments or between different channels from the same experiment. While such correlations certainly exist, e.g. through common Monte Carlo codes or luminosity uncertainties, it is not clear to us how to quantify these effects in a well-defined way. Davier *et al.* [10] claim significant effects, but note that their error from the exclusive channels is very similar to ours (see Table 4 below).

Channel	global $\chi^2_{\min}/\text{d.o.f.}$	globally infl. err.	locally infl. err.	‘global – local’
2π	1.4	3.06	3.09	−0.03
3π	3.0	1.08	0.99	+0.10
$4\pi(2\pi^0)$	1.3	1.19	1.26	−0.07
$4\pi(\text{no } \pi^0)$	1.7	0.49	0.47	+0.02
K^+K^-	1.9	0.57	0.46	+0.11
$K_S^0 K_L^0$	0.8	0.16	0.16	−0.003
$5\pi(1\pi^0)$	1.2	0.09	0.09	0
$6\pi(2\pi^0)$	4.0	0.39	0.24	+0.16

Table 1: Global $\chi^2_{\min}/\text{d.o.f.}$, globally and locally inflated error of a_μ and their difference for several channels. (Range of integration from threshold to 2 GeV.) The five and six pion channels are used as input for our updated isospin analysis (see below).

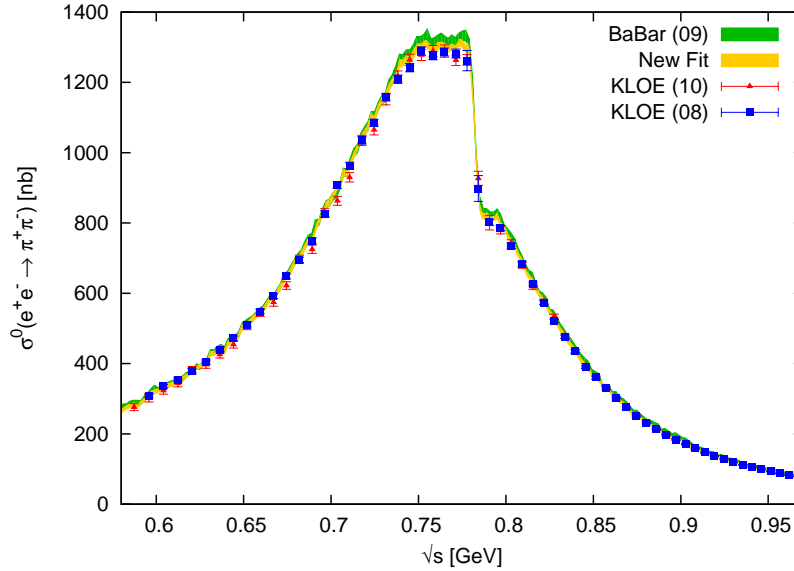


Figure 1: Fit with all data in the 2π channel: light (yellow) band. Radiative return data from BaBar [5] are shown by the darker (green) band, whereas the KLOE [3, 4] data are displayed by the markers as indicated in the plot.

The role of the radiative return data from KLOE and BaBar in the new fit is demonstrated in Fig. 1 in the ρ region from about 0.6 to 0.95 GeV. The new data from BaBar [5] are represented by the darker (green) band, whereas the data from KLOE [3, 4] are displayed by the markers as indicated on the plot. The light (yellow) band is the result of the fit of all combined 2π data, i.e. the data as used in [6] together with the new data from KLOE and BaBar. Figure 2 shows a zoom into the peak region with the $\rho - \omega$ interference and also displays important data from the experiments CMD-2 [11, 12] and SND [13]. Figure 3 displays the low energy region close to threshold, a region previously only sparsely populated by data and where BaBar has added very valuable information. It is clear already from these figures that the KLOE data⁵ are lower

⁵The KLOE08 data are in very good agreement with those of the independent KLOE10 analysis.

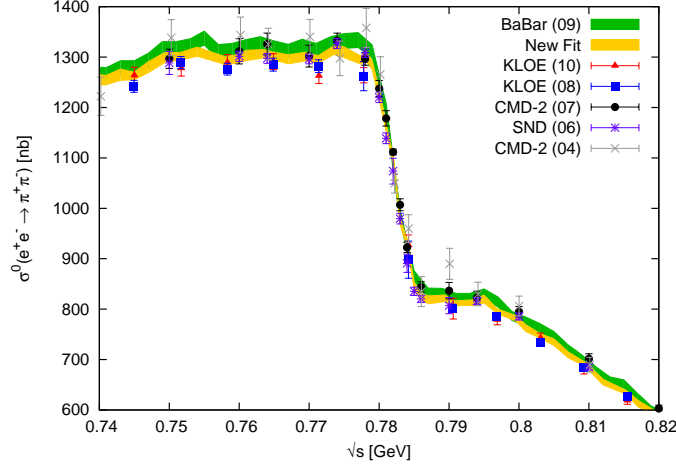


Figure 2: Same as Fig. 1, but ‘zoomed’ in for the $\rho - \omega$ interference region. In addition to the radiative return data, also the important data from CMD-2 [11, 12] and SND [13] are displayed.

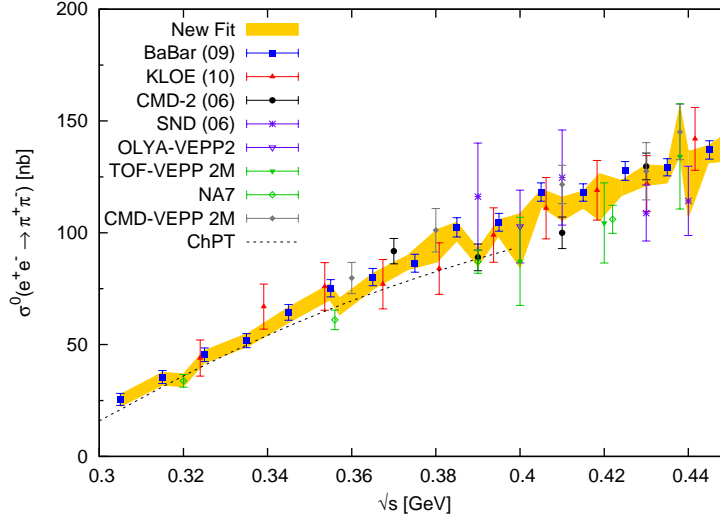


Figure 3: Low energy tail of the $\rho \rightarrow 2\pi$ channel: the light (yellow) band shows the result of our fit using all data, whereas the markers display the actual data points as indicated in the plot. The dashed line represents the prediction of chiral perturbation theory (labelled ChPT) used for the lowest energies from threshold to the first BaBar point at 0.305 GeV.

than the BaBar data, and the fit interpolates between both. Note that despite this tension the fit quality is rather good, with a (global) $\chi^2_{\min}/\text{d.o.f.} = 1.4$. The difference between the KLOE and BaBar data and the full fit to all data is exemplified in Fig. 4, where normalised differences between the sets from radiative return and the fit of all data are displayed as indicated on the plot.

One may ask how stable the fit is with respect to different energy binnings or assumptions on the cross section. There are now a very large number of data points⁶ coming from several different experiments. Thus an extremely fine binning is possible and hence differences, or

⁶We use 879 data points in the 2π channel.

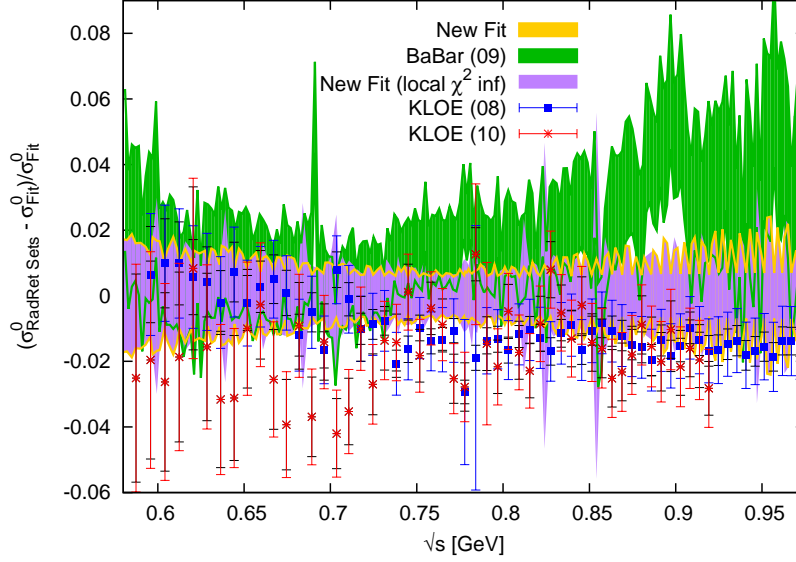


Figure 4: Normalised difference between the data sets based on radiative return from KLOE [3, 4] and BaBar [5] and the fit of all data in the 2π channel, as indicated on the plot. The (lilac) band symmetric around zero represents the error band of the fit given by the diagonal elements of the fit’s covariance matrix, with local error inflation as explained in the text, whereas the light (yellow) band indicates the error band of the fit without inflation.

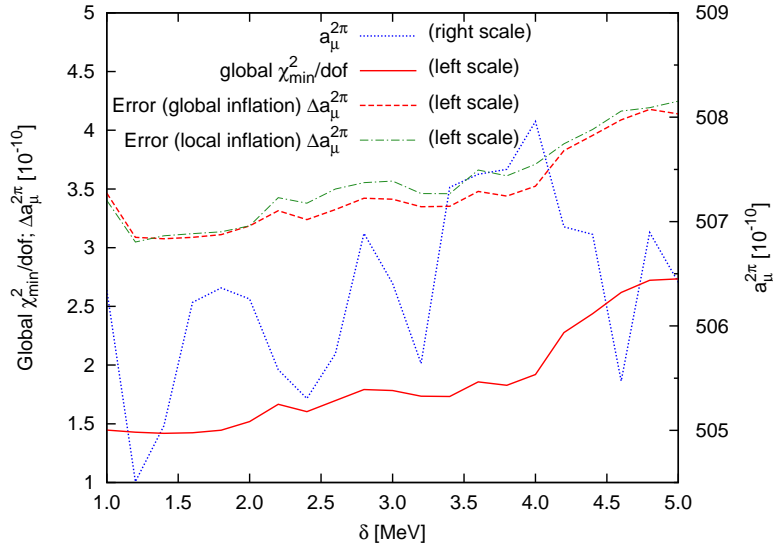


Figure 5: Dependence of the global $\chi^2_{\min}/\text{d.o.f.}$ (solid red line, left scale), the globally inflated error $\Delta a_\mu^{2\pi} \cdot 10^{10}$ (dashed red line, left scale) and the mean value $a_\mu^{2\pi} \cdot 10^{10}$ (dotted blue, right scale) on the choice of the cluster size parameter δ . The dash-dotted green line indicates $\Delta a_\mu^{2\pi} \cdot 10^{10}$ with local error inflation. Recall $a_\mu^{2\pi}$ is the 2π contribution in the range $0.305 < \sqrt{s} < 2$ GeV.

biases, due to varying the underlying model for the cross section are negligible.⁷ However, there is a remaining dependence on the way the data are binned. For the current analysis,

⁷As we have checked and discussed in [2], our simple assumption of a piecewise constant cross section in the energy bin and simple trapezoidal integration are well justified.

we have further refined our algorithm to ‘cluster’ the data in energy bins with a given target cluster size δ . Compared to the original algorithm used in [2], we now allow for more flexible bin-sizes in regions of very dense or sparse data.⁸ The dependence on the target cluster size δ is displayed in Fig. 5 for a range of $1 \text{ MeV} < \delta < 5 \text{ MeV}$: the solid (red) line gives $\chi^2_{\min}/\text{d.o.f.}$, the dashed (red) line the error of the resulting 2π contribution to a_μ (after error inflation and in units of 10^{-10}) and the dotted (blue) line shows the variation of the mean value of $a_\mu^{2\pi}$ (again in units of 10^{-10}). This demonstrates that, (i) data clustering with cluster sizes δ up to about 2 MeV is advantageous as the fit quality is maintained and the error reduced, (ii) larger clustering is disfavoured by an increase in $\chi^2_{\min}/\text{d.o.f.}$ which overcompensates any possible additional gain of the error before error inflation, (iii) the mean value of the resulting $a_\mu^{2\pi}$ varies by about 1σ , depending on the particular choice of the clustering. We have chosen $\delta = 1.5 \text{ MeV}$ which leads to the best fit quality, the smallest error and a mean value of $a_\mu^{2\pi}$ right in the middle of the band of possible results for various clustering choices. With this we obtain

$$a_\mu^{2\pi}(0.32 - 2 \text{ GeV}) = (504.23 \pm 2.97) \cdot 10^{-10} \quad (4)$$

for the energy range $0.32 < \sqrt{s} < 2 \text{ GeV}$ (note Fig. 5 is for the different interval $0.305 < \sqrt{s} < 2 \text{ GeV}$). This result is to be compared to the result without the radiative return data (337 points from BaBar, 60 from KLOE08 and 75 from KLOE10), for which we would get

$$a_\mu^{2\pi, \text{w/out Rad. Ret.}}(0.32 - 2 \text{ GeV}) = (501.26 \pm 4.48) \cdot 10^{-10},$$

if the same small clustering size $\delta = 1.5 \text{ MeV}$ is used. The inclusion of the data from radiative return leads therefore to a considerable pull-up of our previous result. Even more, without the many data points from BaBar and KLOE the fit would prefer the much bigger cluster size of 4.2 MeV (as used in [6]), for which we would get

$$a_\mu^{2\pi, \text{w/out Rad. Ret.}}(0.32 - 2 \text{ GeV}) = (498.65 \pm 3.28) \cdot 10^{-10}. \quad (5)$$

The observed significant pull-up of $a_\mu^{2\pi}$ is expected from Fig. 4, and similar effects from the inclusion of radiative return data have been reported in [14]. Given the small error of the new data based on radiative return, the gain in accuracy seems modest. However, this is a consequence of the tension between the different data sets as discussed above.

It is interesting to compare $a_\mu^{2\pi}$ in the restricted energy range where the KLOE (and BaBar) data overlap with the other data. In the range $0.5958 < \sqrt{s} < 0.9192 \text{ GeV}$ the $a_\mu^{2\pi}$ (in units of 10^{-10}) using the KLOE08 data gives 376.3 ± 3.4 , in fair agreement with KLOE10 for which we get 373.4 ± 3.3 , whereas using the BaBar data results in 384.4 ± 2.8 . In the same range and using our original choice of $\delta = 4.2 \text{ MeV}$, the integral over the compilation of all other (excluding radiative return) data yields 376.0 ± 2.6 . A weighted average of these numbers would result in a prediction of 377.9 ± 1.5 . In comparison, combining all sets before integration in this energy range gives 380.0 ± 2.2 . As expected from the discussion of the full energy range, this result is considerably higher; and the larger error is a direct consequence of the tension between

⁸This adaptive clustering avoids individual bins containing too many data points, and prevents points very close to each other from being forced into different bins, as could happen with a fixed cluster size δ .

the various sets, which would be partly masked if the combination is done after integration. Therefore, for our updated SM prediction of $g - 2$ given below, we will use all 2π data in the same way, i.e. combine them before integration and use Eq. (4) for the 2π contribution.

Note that for our compilation of the hadronic cross section, and in particular for the 2π channel, we do not use spectral function data from hadronic τ decays, but prefer to entirely rely on $e^+e^- \rightarrow$ hadrons cross sections. Considerable effort has been invested in model-based estimates of the isospin breaking corrections needed to translate $\tau \rightarrow \nu_\tau W \rightarrow \nu_\tau \pi \pi^0$ ($I = 1$) spectral function data into the $e^+e^- \rightarrow \gamma^* \rightarrow \pi^+\pi^-$ cross section.⁹ However, even after application of the known isospin breaking corrections, differences between the two quantities remain. In their recent works [16, 10], Davier *et al.* have found, compared to their earlier studies, a diminished, though still sizeable discrepancy between the isospin rotated τ data from ALEPH, OPAL, CLEO and BELLE, and the e^+e^- data. This is at variance with results from Benayoun *et al.*, who found agreement of the τ with the e^+e^- data in an analysis based on hidden local symmetry and dynamical (ρ, ω, ϕ) mixing [17]. In a very recent work, Jegerlehner and Szafron [18] study the effect of $\rho - \gamma$ mixing, which is absent in the τ spectral function, but can be estimated from the e^+e^- data. They find that after including these effects the τ spectral function data confirm the e^+e^- data and are very close to them, but lead only to a marginal improvement in the accuracy of a_μ^{had} . A detailed discussion of these issues goes beyond the scope of this work. However it is fair to say that there are still many open questions. Given the limited understanding of the hadronic dynamics and the resulting model dependence of the isospin breaking corrections, and given the small influence of the τ data, we, at present, do not include them for the best possible prediction of $g - 2$.

2.2 The energy region below 2 GeV

Another region, where important changes have occurred through new data, is the energy region between 1.43 and 2 GeV. This region is particularly difficult, as, compared to lower energies, many more multi-hadron exclusive final states are open and have to be included to obtain an accurate prediction of σ_{had} . However, this energy range has been inaccessible for recent experiments measuring low energy hadronic cross sections, especially CMD-2 and SND operating at VEPP-2M in Novosibirsk.¹⁰ Hence the quality of the available data was not very good, with some channels hardly constrained at all. Alternatively, one can rely on inclusive R measurements, but also for these only rather old and not very precise data are available, with poorly constrained systematics and limited statistics. The situation has recently changed significantly, with BaBar measuring, again through the method of radiative return, many channels with higher accuracy than earlier experiments. These include new measurements of the channels $2\pi^+2\pi^-$ [20], $K^+K^-\pi^0$, $K_S^0K\pi$ [21], $2\pi^+2\pi^-\pi^0$, $K^+K^-\pi^+\pi^-\pi^0$, $2\pi^+2\pi^-\eta$ [22], $2\pi^+2\pi^-2\pi^0$

⁹The $I = 0$ part, which is not present in the τ decays, contributes about 25% to $a_\mu^{2\pi}$ and has to be estimated from e^+e^- data, which contain the coherent sum of both $I = 1$ and $I = 0$ contributions. (See [15] for a recent evaluation of $\rho - \omega$ mixing contributions and its model dependence.)

¹⁰This will change in the near future, with the experiments CMD-3 and SND already taking data at the upgraded VEPP-2000 collider, see [19].

[23], all of which we use for this updated analysis.¹¹

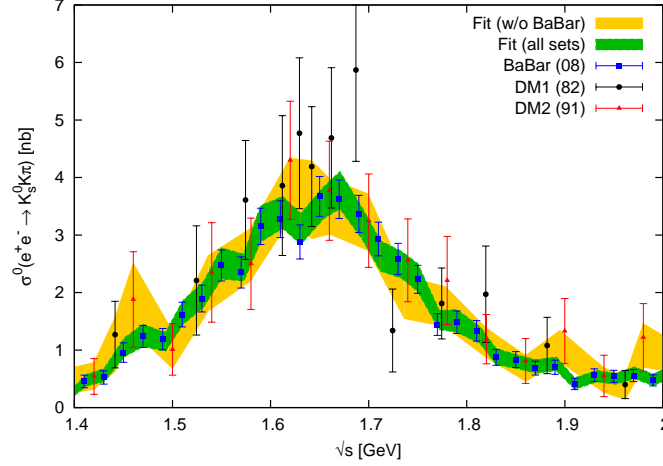


Figure 6: $K_S^0 K \pi$ channel with improvement due to recent BaBar data [21] from radiative return.

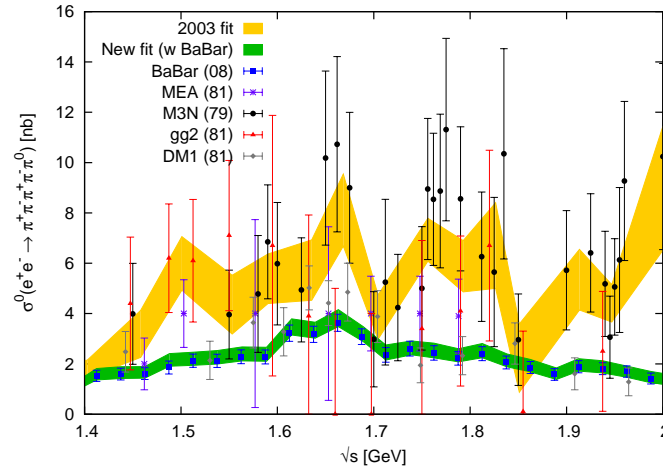


Figure 7: $2\pi^+2\pi^-\pi^0$ channel with data from BaBar [23]. The data from M3N are not taken into account in the new fit.

Figures 6 – 9 exemplify the influence of the new BaBar data in the compilations for the subleading channels $K_S^0 K \pi$, $2\pi^+2\pi^-\pi^0$, $2\pi^+2\pi^-$ and $2\pi^+2\pi^-2\pi^0$. In all these figures the light (yellow) bands indicate our older compilations without the recent BaBar data, whereas the darker (green) bands show the results of our new fits. The most important data are displayed by markers as indicated in the plots. (For full references to older data see [2, 6].) Note that the new data from BaBar now allow us to discard older, not very precise data from M3N (in the 5π and 6π channels) and from DM2 (5π), which were only available from theses and which are not compatible with the new measurements. In the $2\pi^+2\pi^-\pi^0$ channel we have also included data from DM1 [25], with properly added non-resonant contributions. All the channels shown here are now somewhat dominated by the radiative return measurements from BaBar. Only in the $2\pi^+2\pi^-2\pi^0$ channel do other data still influence the fit in a significant way through a slight adjustment via the fitted renormalisation factors f_k of the χ^2 minimisation.

¹¹A partial update of our analysis in this region has already been reported at the PhiPsi09 conference [24].

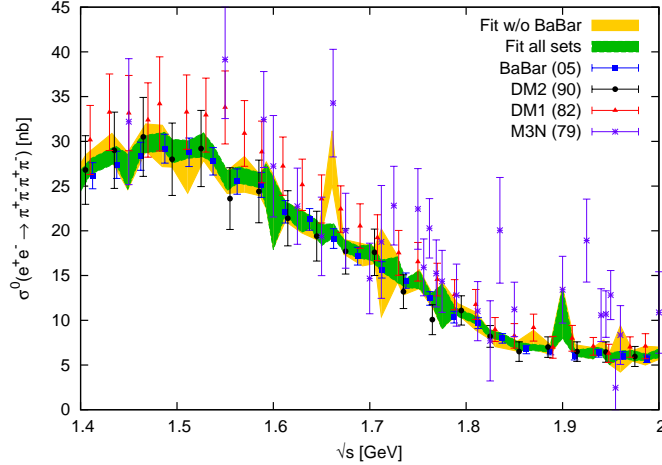


Figure 8: $2\pi^+2\pi^-$ channel with data from BaBar [20].

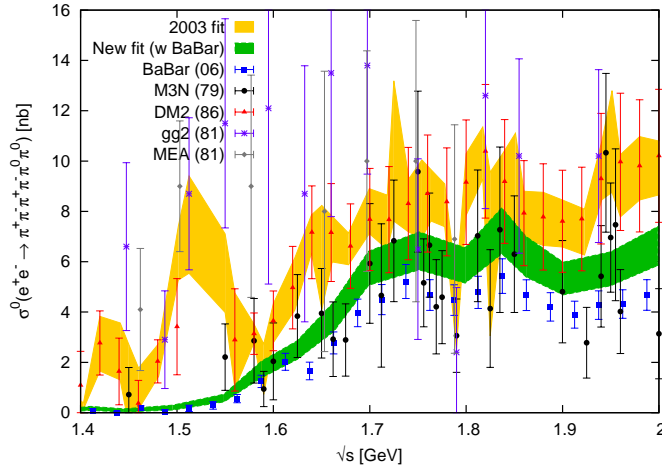


Figure 9: $2\pi^+2\pi^-2\pi^0$ channel with data from BaBar [23]. The data from M3N and DM2 are not taken into account in the new fit.

As is clear from figures 6 – 9, the new data are not always in agreement with earlier measurements. In case of disagreement of different data sets, the fit has a bad (global) $\chi^2_{\min}/\text{d.o.f.}$. As done throughout our analysis, in such cases the error of the channel's contribution to a_μ (and $\Delta\alpha$) is scaled up by applying local error inflation through χ^2 values calculated in each cluster of the data compilation. This happens, for example, in the $2\pi^+2\pi^-2\pi^0$ channel where $\chi^2_{\min}/\text{d.o.f.} = 2.7$, but see Table 1 for details.

Even after the many improvements due to data from BaBar, there are still subleading channels where we have only poor or no data at all, and where the sum of exclusive channels (for energies below 2 GeV) requires the use of isospin relations. We have updated the isospin relations used in our earlier analysis [2] along the lines of [10] and also taking into account the latest data from BaBar [26].¹² The results for the contributions to a_μ from the channels

¹²Contrary to the original analyses, in the 5π and 6π channels the contributions from η decays are excluded, and new channels $\eta\omega$ and $\eta\phi$ are taken into account, which are now also used in the isospin relations. We calculate the contributions from $\eta\omega$ with the help of a Breit-Wigner parametrisation, as a data tabulation is not available to us.

Channel	This work	HMNT (03) [2]	approach used in [2]
$K\bar{K}\pi$	2.77 ± 0.15	2.58 ± 0.26	sum of $K^+K^-\pi^0$, $K_{S,L}^0K\pi$, $K_S^0K_L^0\pi^0$
$K\bar{K}2\pi$	3.31 ± 0.58	3.63 ± 1.24	different relation based on channel K_S^0X
$K\bar{K}3\pi$	0.08 ± 0.04	-	not accounted for
$\omega(\rightarrow \pi^0\gamma)K\bar{K}$	0.01 ± 0.00	-	not accounted for
$2\pi^+2\pi^-\pi^0$ (no η)	1.20 ± 0.10	2.85 ± 0.25	purely data-based incl. η
$\pi^+\pi^-3\pi^0$ (no η)	0.60 ± 0.05	1.19 ± 0.33	based only on M3N data
$\omega(\rightarrow \pi^0\gamma)2\pi$	0.11 ± 0.02	0.07 ± 0.01	only $\omega(\rightarrow \pi^0\gamma)\pi^+\pi^-$ based on data
$2\pi^+2\pi^-2\pi^0$ (no η)	1.80 ± 0.24	3.32 ± 0.29	purely data based, incl. η
$\pi^+\pi^-4\pi^0$ (no η)	0.28 ± 0.28	0.12 ± 0.12	different relation, incl. η
$\omega(\rightarrow \pi^0\gamma)3\pi$	0.22 ± 0.04	-	not estimated
$\eta\pi^+\pi^-$ (data)	0.98 ± 0.24	0.49 ± 0.07	$\eta \rightarrow 3\pi$ excluded
$\eta\omega$ (data)	0.42 ± 0.07	n/a	no data, not estimated separately
$\eta\phi$ (data)	0.46 ± 0.03	n/a	no data, not estimated separately
$\eta 2\pi^+2\pi^-$ (data)	0.11 ± 0.02	n/a	no data, not estimated separately
$\eta\pi^+\pi^-2\pi^0$	0.11 ± 0.06	n/a	not estimated separately
Total	12.46 ± 0.76	14.25 ± 1.46	

Table 2: Contributions to a_μ from exclusive channels for energies up 2 GeV, estimated using isospin relations following [10] and as discussed in the text. For comparison also the results of our original analysis are given.

estimated in this way are given in Table 2, where for comparison also the numbers used for our original analysis [2] are shown.¹³ Note that the sum of these contributions in the energy range from 1.43 to 2 GeV has gone down by nearly two units in 10^{-10} , mainly as a consequence of using new BaBar data in the $2\pi^+2\pi^-\pi^0$ and the $2\pi^+2\pi^-2\pi^0$ channels as shown in Figs. 7 and 9. (The use of the new, more complicated isospin relations for the multi-pion states has only a minor influence.) Compared to earlier analyses, recent data from BaBar for the $K\bar{K}\pi$, $K\bar{K}2\pi$ and $K\bar{K}3\pi$ channels have allowed us to avoid the use of the rather badly constrained semi-inclusive channel K_S^0X . This has resulted in a much improved error (by more than a factor of two) of the contribution from the $K\bar{K}2\pi$ channel. This channel is dominating the error in the energy region just below 2 GeV, which leads to a significant error reduction as given in the last line of Table 2. In future, data from VEPP-2000 in this energy range will provide important cross-checks for these channels and will hopefully lead to a further reduction of the error of a_μ .

Note that in our previous $g-2$ analyses [2, 6] we used two alternative treatments to calculate the contributions in the 1.43–2 GeV energy interval. We *either* added up the contributions from all the exclusive channels, *or* simply used a combination of the available data on the inclusive cross section, $\sigma(e^+e^- \rightarrow \text{all hadrons})$. There was a discrepancy between the two methods. The inclusive data were lower than the sum of the exclusive channels, though they were found to be similar in shape. Our updated analysis shows similar findings. This is demonstrated

¹³M3N data in the $\pi^+\pi^-3\pi^0$ channel, which were used in our original channel compilation, are discarded in this analysis, and the $\pi^+\pi^-3\pi^0$ contribution is now estimated by isospin relations.

in Fig. 10, where our compilation for $R_{\text{had}}(s) = \sigma_{\text{had}}^0(s)/(4\pi\alpha^2/(3s))$ from the old inclusive data is compared to the sum of the exclusive channels as indicated on the plot and in the caption. The shaded band displays our new compilation of the sum of the exclusive channels, which is more accurate, and, for energies up to about 1.8 GeV, slightly lower than our older compilation (as used in [2]) which is shown by the overlaid dashed (blue) curves. In our analysis

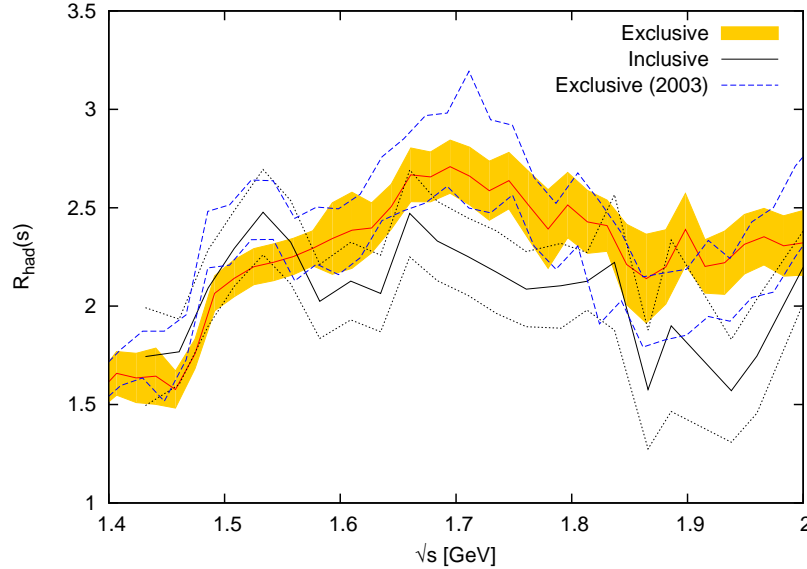


Figure 10: Comparison of our combination of inclusive data with the sum of exclusive channels in the energy region below 2 GeV. The shaded band, with the solid (red) line indicating the mean value, gives our updated compilation including the new data sets from BaBar; the band formed by the two dashed (blue) curves shows our old result used in [2]. The compilation of the old inclusive measurements (solid and dotted black lines for mean value and error) has a similar energy dependence but is significantly lower over most of the energy range.

[2] the difference in a_μ between using the ‘exclusive’ and the ‘inclusive’ option was $3.8 \cdot 10^{-10}$, corresponding to about one standard deviation in a_μ in the energy interval $1.43 < \sqrt{s} < 2$ GeV. Quite a few channels were very poorly constrained by experiment, and for some channels estimates based on isospin relations had to be used as no data were available at all. At this point we had invoked a QCD sum-rule analysis, relating the convolution integral of $R_{\text{had}}(s)$ with a suitable kernel function $f(s)$ to a corresponding contour-integral of the perturbatively calculated Adler- D function¹⁴,

$$\int_{s_{\text{thr}}}^{s_0} ds R_{\text{had}}(s) f(s) = \int_C ds D(s) g(s), \quad (6)$$

with $f(s) = (1 - s/s_0)^m (s/s_0)^n$; C is a circular contour of radius s_0 and $g(s)$ is a known function once $f(s)$ is specified (see [2] for formulae and details). We then found that the inclusive data were more compatible with perturbative QCD and the world-average of α_s . Therefore we had preferred to quote the result obtained from using the inclusive data in this energy region.

¹⁴Earlier work along these lines can be found in [27].

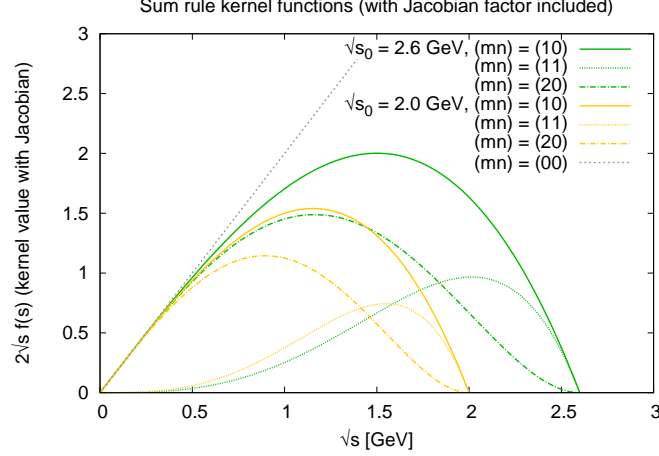


Figure 11: Kernel function $f(s)$, multiplied by the Jacobian factor $2\sqrt{s}$, as a function of \sqrt{s} for different choices of the parameters m , n and $\sqrt{s_0}$, as indicated on the plot.

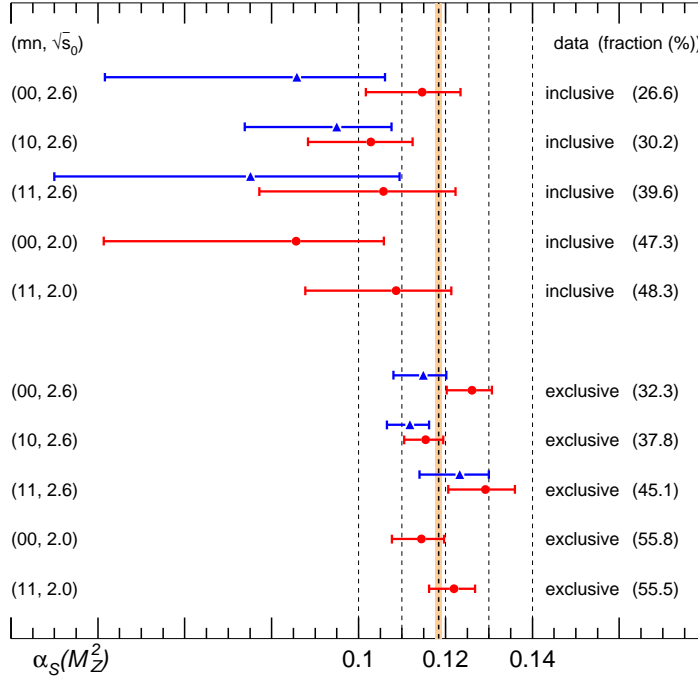


Figure 12: Sum-rules, (6), with different values of m , n and $\sqrt{s_0}$, translated into a prediction of α_s (see [2] for details). Upper part: use of inclusive data in the region $1.43 < \sqrt{s} < 2$ GeV, lower part: use of our up-dated compilation for the sum of exclusive data in the same energy interval. The (red) circles show the results based on data alone for the left hand side of (6), whereas for the (blue) triangles perturbative QCD has been used in the region above 2 GeV, see subsection 2.4, in particular Fig. 15. The slim (orange) band shows the world-average of $\alpha_s(M_Z^2)$. Also listed are the fractions with which the energy region $1.43 < \sqrt{s} < 2$ GeV contributes to the respective sum-rules.

In light of the significant changes of the data we have now repeated the sum-rule analysis. For the Adler- D function we now use the full four-loop result [28], which had not been available for our original analysis. It is informative to show a range of sum-rules, although they are highly correlated. The sensitivity of the different sum-rules w.r.t. the energy range is demonstrated in Fig. 11, where different kernel functions $f(s)$ (multiplied by the Jacobian factor) are displayed as a function of the energy \sqrt{s} . The new results are displayed in Fig. 12, where different sum-rules based on the Adler- D function from pQCD are made to match the corresponding sum-rule integrals over the data by fitting α_s as a free parameter. (Note that the error bars for the sum-rule results represent only the statistical and systematic errors from the experimental data used in our data compilations. These errors are large compared to the uncertainty from pQCD when estimated by comparing the results based on four-loop QCD with those at three-loop accuracy.) The band displays the current world average for $\alpha_s(M_Z^2) = 0.1184 \pm 0.0007$ [29]. Compared to our previous analysis in 2003, the sum-rules do not favour the inclusive data any more, but tend to prefer the more precise exclusive data. Note that this is partly a consequence of the recent changes of the low energy (mainly the ρ region) and higher energy (above 2 GeV) data common to both options, and partly due to the change of the data in the range between 1.43 and 2 GeV. (The fraction of the sum-rule stemming from this region is indicated in brackets in Fig. 12.) As a result of these sum-rule observations, and bearing in mind the recent improvements of the exclusive data, we are led to use, in the energy range from 1.43 to 2 GeV, the sum over the exclusive data for our compilation of $g - 2$ and $\Delta\alpha$.¹⁵ This

¹⁵Also note that, in the region just below 2 GeV, the sum of the exclusive channels is in better agreement

Channel	This work	HMNT (03) [2]	Difference
$\pi^+\pi^-\pi^0\pi^0$	10.80 ± 0.77	10.84 ± 0.73	-0.04
$2\pi^+2\pi^-$	8.64 ± 0.28	8.61 ± 0.30	$+0.03$
$5\pi, 6\pi$ (incl. η)	5.92 ± 0.41	7.65 ± 0.43	-1.73
$K\bar{K}\pi$	2.69 ± 0.15	2.48 ± 0.23	$+0.21$
$K\bar{K}2\pi$	3.31 ± 0.58	3.63 ± 1.32	-0.32
$\pi^+\pi^-\pi^0$	1.25 ± 0.07	0.61 ± 0.09	$+0.64$
Others	1.99 ± 0.17	1.86 ± 0.56	$+0.13$
Sum of excl.	34.61 ± 1.11	35.68 ± 1.71	-1.07
Inclusive	31.99 ± 2.43	31.91 ± 2.42	$+0.08$
weighted avg.	34.15 ± 1.10		

Table 3: Contributions to a_μ from the most important channels in the region from 1.43 to 2 GeV. The numbers given in the second column (‘This work’) are our new results based on the updated compilation, whereas the column labelled ‘HMNT (03)’ refers to our old analysis [2]. The last column gives the difference, which, due to changes in the treatment of radiative corrections, is also present in the combination of the inclusive data, for which no new data sets are available. The last three lines give the different options for use of data in this region: sum of exclusive channels (our preferred choice), inclusive data, or the weighted average. (All values in units of 10^{-10} .)

does lead to a considerable (by a factor of two) improvement of the error in this region but also results in a noticeable shift upwards of the contributions to a_μ and $\Delta\alpha$ (about $+3 \cdot 10^{-10}$ for a_μ) compared to our previous analyses. (However, note that if we were to average the inclusive and the sum over exclusive, both the result and the error would change only marginally w.r.t. using exclusive data only in this region, as quantified in Table 3.)

The numerical results are summarised in Table 3, where we display the channels with the largest contributions and the largest changes in this region. The row labelled ‘Others’ is the sum of all contributions not listed explicitly. It is clear that, although the difference between the sum of exclusive and the inclusive data has not changed dramatically, the new sum of exclusive channels, with many improvements due to data from BaBar, is considerably more accurate than the old inclusive data.

2.3 Changes in other channels

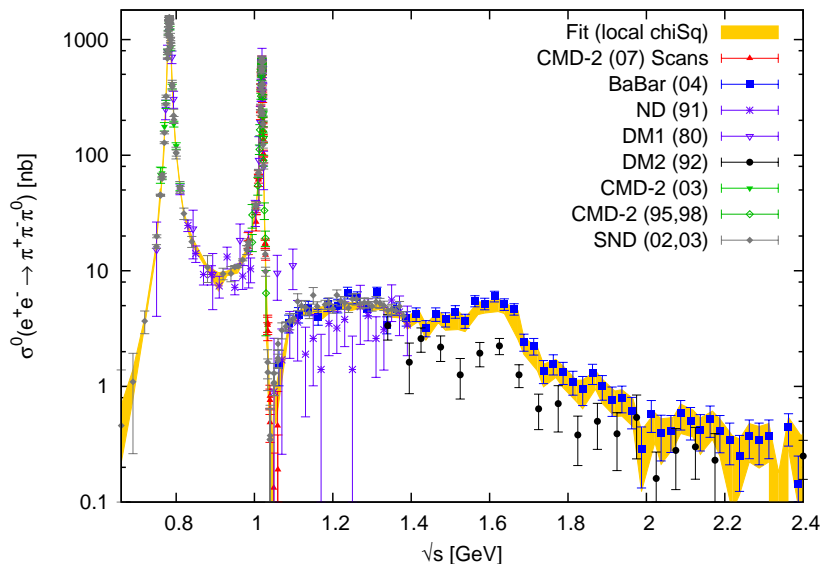


Figure 13: $\pi^+\pi^-\pi^0$ channel with ω and ϕ resonances.

In addition to the important improvements in the 2π channel and in the region just below 2 GeV discussed above, there have also been a number of changes in other channels. Compared to [6] we have included the following data sets: K^+K^- from CMD-2 [30] and SND [31], $K_S^0K_L^0$ from SND [32], $\pi^+\pi^-\pi^0$ from CMD-2 [33], $\omega\pi^0$ from KLOE [34], and inclusive R data at higher energies above 2 GeV from BES [35, 36] and CLEO [37]. The new data from CMD-2 and SND have further consolidated and improved the narrow ω and ϕ resonances, whose contributions can be reliably predicted by direct integration of the data (as opposed to fits using a specific parametrisation of the resonance). Figure 13 shows the 3π channel with the ω and ϕ resonances, whereas the ϕ resonance in the K^+K^- channel is displayed in Fig. 14.

In Table 4 we compare our predictions of the contributions to a_μ from the exclusive channels up to 1.8 GeV with the results as given in [10]. While the agreement of the sum of all contributions with the prediction from pQCD than the inclusive data. However, we do not use pQCD in this energy region.

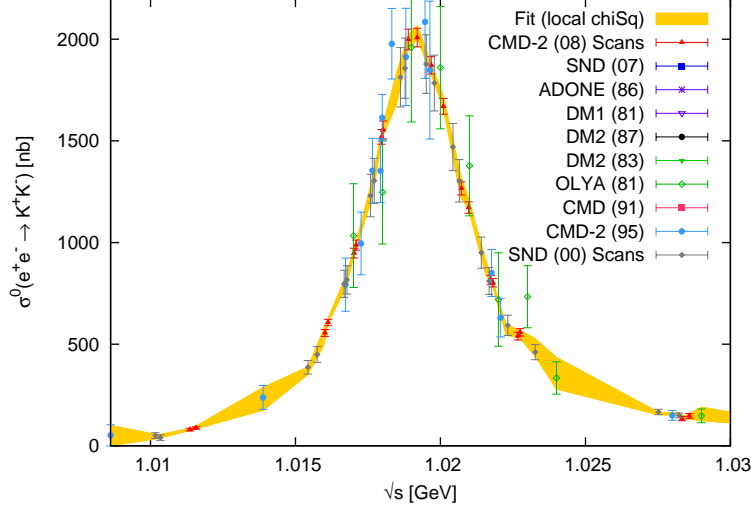


Figure 14: ϕ resonance in the K^+K^- channel.

Channel	This work	DHMZ (10) [10]	Difference
$\eta\pi^+\pi^-$	0.88 ± 0.10	1.15 ± 0.19	-0.27
K^+K^-	22.09 ± 0.46	21.63 ± 0.73	0.46
$K_S^0 K_L^0$	13.32 ± 0.16	12.96 ± 0.39	0.36
$\omega\pi^0$	0.76 ± 0.03	0.89 ± 0.07	-0.13
$\pi^+\pi^-$	505.65 ± 3.09	507.80 ± 2.84	-2.15
$2\pi^+2\pi^-$	13.50 ± 0.44	13.35 ± 0.53	0.15
$3\pi^+3\pi^-$	0.11 ± 0.01	0.12 ± 0.01	-0.01
$\pi^+\pi^-\pi^0$	47.38 ± 0.99	46.00 ± 1.48	1.38
$\pi^+\pi^-2\pi^0$	18.62 ± 1.15	18.01 ± 1.24	0.61
$\pi^0\gamma$	4.54 ± 0.14	4.42 ± 0.19	0.12
$\eta\gamma$	0.69 ± 0.02	0.64 ± 0.02	0.05
$\eta 2\pi^+2\pi^-$	0.02 ± 0.00	0.02 ± 0.01	0.00
$\eta\omega$	0.38 ± 0.06	0.47 ± 0.06	-0.09
$\eta\phi$	0.33 ± 0.03	0.36 ± 0.03	-0.03
$\phi(\rightarrow \text{unaccounted})$	0.04 ± 0.04	0.05 ± 0.00	-0.01
Sum of isospin channels	5.98 ± 0.42	6.06 ± 0.46	-0.08
Total	634.28 ± 3.53	633.93 ± 3.61	0.35

Table 4: Contributions to a_μ (in units of 10^{-10}) in the energy region from 0.305 to 1.8 GeV from exclusive channels: Results based on the data compilation as used in this analysis compared to the results as given by Davier *et al.* [10].

tributions is very good, there are differences in several channels, which are of the order of the errors, notably in the 2π , 3π and the KK channels. These differences presumably come from a different treatment of the data, like radiative corrections and the clustering and integration procedure, and reflect the different choices made by different groups.

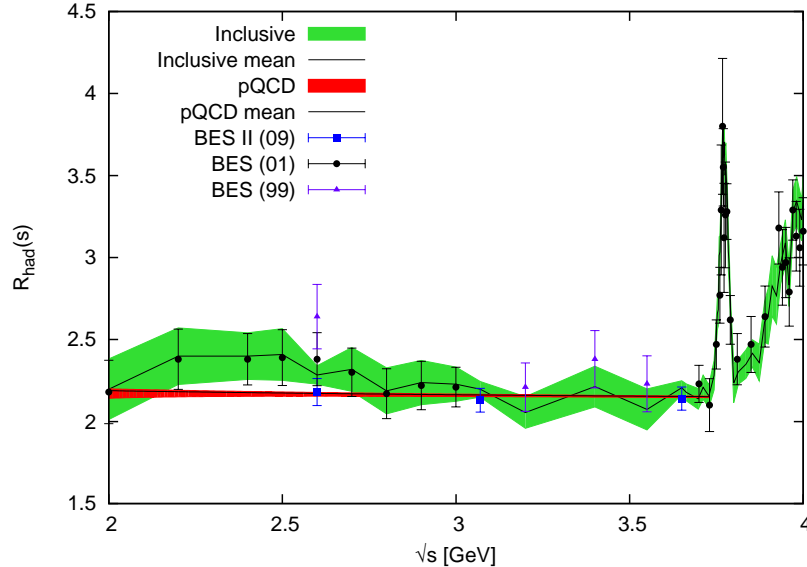


Figure 15: Compilation of inclusive data (light (green) band) above 2 GeV compared to the prediction of pQCD (dark (red) band). The peaked structure is the $\psi(3770)$, very close to the open charm threshold. The J/ψ and ψ' are not resolved by these data but are included separately as narrow resonances in our analysis.

2.4 Region above 2 GeV

Of particular interest is the region of inclusive data above 2 GeV. Although its influence for $g-2$ is suppressed by the kernel function K of (2), the new data lead to a significant shift downwards of the hadronic contributions to $g-2$ from this energy region. (The direct integration of our new data compilation in the energy range $2 < \sqrt{s} < 11.09$ GeV gives an a_μ contribution lower by about $1.4 \cdot 10^{-10}$ compared to our earlier result in [6]). In Fig. 15 the new fit and some of the important data are compared to pQCD. It is intriguing that the newest data from BES [36], which are responsible for the pull-down in this region, are in perfect agreement with the predictions from pQCD, which in turn are considerably lower than the data in the region around 2.4 GeV. It is interesting to replace data by pQCD above 2 GeV in the sum-rule analysis. We have done so by employing the latest version of the routine `rhad` [38] which includes recently obtained four-loop contributions, and by leaving α_s as a free parameter in the sum-rule analysis. Our results are displayed in Fig. 12 as (blue) triangles, which are, as expected, lower than the respective results based on data alone. The sum-rule integrals, expressed in terms of $\alpha_s(M_Z^2)$, now show a slightly improved agreement with the world-average for the exclusive data, and an even worse agreement if inclusive data are used. Nevertheless, for our data-driven analysis of $g-2$ and $\Delta\alpha$, we use the data in the region from 2 to 2.6 GeV. However, between 2.6 and 3.73 GeV we do use pQCD, but with an inflated error determined by the percentage errors of the BES data [36].¹⁶ From 11.09 GeV we use pQCD as done already in [2]. The data in this region

¹⁶If we would use pQCD also from $2 < \sqrt{s} < 2.6$ GeV and estimate the error from the pQCD uncertainty, the contribution to a_μ from this region would be $(14.49 \pm 0.13) \cdot 10^{-10}$ instead of $(15.69 \pm 0.63) \cdot 10^{-10}$. If we would use (inclusive) data instead of pQCD from $2.6 < \sqrt{s} < 3.73$ GeV, our prediction for a_μ would be larger by about $0.2 \cdot 10^{-10}$ with a marginally increased error. Using pQCD instead of data at higher energies above

is very poor and pQCD, above the open bottom threshold, is very well justified. Note that, as in [2, 6], the narrow resonances J/ψ , ψ' and the $\Upsilon(1-6S)$ are added separately as they are not resolved by the data used in the inclusive compilation.

2.5 $a_\mu^{\text{had, LO VP}}$ and $a_\mu^{\text{had, HO VP}}$

Table 5 gives the contributions to the leading order hadronic vacuum polarisation from different energy ranges, including different options for the region from 1.43 to 2 GeV, and makes the comparison with our earlier results from [6]. From the fourth column it is clear that the changes

Contribution	This work	HMNT (06) [6]	Difference
$2m_\pi - 0.32 \text{ GeV}$ (ChPT, 2π)	2.36 ± 0.05	2.36 ± 0.05	± 0.00
$3m_\pi - 0.66 \text{ GeV}$ (ChPT, 3π)	0.01 ± 0.00	0.01 ± 0.00	± 0.00
$m_\pi - 0.60 \text{ GeV}$ (ChPT, $\pi^0\gamma$)	0.13 ± 0.01	0.13 ± 0.01	± 0.00
$m_\eta - 0.69 \text{ GeV}$ (ChPT, $\eta\gamma$)	0.00 ± 0.00	0.00 ± 0.00	± 0.00
$\phi \rightarrow \text{unaccounted modes}$	0.04 ± 0.04	0.06 ± 0.06	-0.02
$0.32 - 1.43 \text{ GeV}$	606.50 ± 3.35	601.96 ± 3.19	$+4.54$
$1.43 - 2 \text{ GeV}$ (excl. only)	34.61 ± 1.11	36.38 ± 1.66	-1.77
$1.43 - 2 \text{ GeV}$ (incl. only)	31.99 ± 2.43	32.05 ± 2.43	-0.06
$1.43 - 2 \text{ GeV}$ (incl.-excl. avg.)	34.15 ± 1.10	n/a	n/a
$2 - 11.09 \text{ GeV}$	41.19 ± 0.82	42.75 ± 1.08	-1.56
$J/\psi + \psi'$	7.80 ± 0.16	7.90 ± 0.16	-0.10
$\Upsilon(1S - 6S)$	0.10 ± 0.00	0.10 ± 0.00	± 0.00
$11.09 - \infty$ (pQCD)	2.11 ± 0.00	2.11 ± 0.00	± 0.00
Sum (excl.-excl.-incl.)	694.86 ± 3.71	693.77 ± 3.84	$+1.09$
Sum (excl.-incl.-incl.)	692.25 ± 4.23	689.44 ± 4.17	$+2.81$
Sum (excl.-avg.-incl.)	694.40 ± 3.67	n/a	n/a

Table 5: Contributions to $a_\mu^{\text{had, LO VP}}$ obtained in this work compared to the values used in our analysis [6]. The last column gives the differences. (All values in units of 10^{-10} .) The first four lines give our predictions of contributions close to threshold where no data are available and are based on chiral perturbation theory (ChPT), see [2] for details. For $2.6 < \sqrt{s} < 3.73 \text{ GeV}$ pQCD with errors comparable to those of the latest BES data is used as default for this work, see the discussion in the text. The different choices quoted in the last three lines refer to the energy regions below 1.43 GeV, for $1.43 < \sqrt{s} < 2 \text{ GeV}$ and above.

w.r.t. our analysis from 2006 partially cancel each other. However, the inclusion of the radiative return data from KLOE and BaBar, and taking into account the exclusive data in the region from 1.43 to 2 GeV, dominates the changes and leads to a slightly increased prediction of $a_\mu^{\text{had, LO VP}}$ of

$$a_\mu^{\text{had, LO VP}} = (694.91 \pm 3.72_{\text{exp}} \pm 2.10_{\text{rad}}) \cdot 10^{-10}. \quad (7)$$

the charm resonance region but below the bottom threshold would lead to a negligible change in a_μ .

The first error, labelled ‘exp’, stems from the statistical and systematic errors of the experimental data, as used in our combination procedure. The second, additional error, labelled ‘rad’, is due to uncertainties in the application of radiative corrections to the data. For a detailed discussion of its estimate see [2]. Note that the value given in (7) slightly differs from the one quoted in Table 5, for which the 2π data were used from 0.32 GeV to facilitate the comparison with [6]. For our new prediction (7), the 2π data are used from 0.305 GeV and only below this chiral perturbation theory is applied.

With the same data compilation we can also determine the higher order VP contributions, see [2] for details concerning the corresponding dispersion integrals. Our new value is only slightly changed from our previous prediction and reads

$$a_{\mu}^{\text{had, HO VP}} = (-9.84 \pm 0.06_{\text{exp}} \pm 0.04_{\text{rad}}) \cdot 10^{-10}. \quad (8)$$

Equations (7) and (8) are used for our updated prediction of $g - 2$. These results, together with (14), are the main results of this paper.

3 Standard Model Prediction of $g - 2$

For the Standard Model prediction of $(g - 2)_{\mu}$, contributions from all sectors have to be added:

$$a_{\mu}^{\text{SM}} = a_{\mu}^{\text{QED}} + a_{\mu}^{\text{EW}} + a_{\mu}^{\text{had}}. \quad (9)$$

In contrast to the hadronic sector, both QED and electro-weak (EW) contributions can be calculated reliably using perturbation theory. After many years’ work the QED contributions are known to full four-loop accuracy, and estimates for the five-loop contributions are ongoing (see e.g. the recent works [39, 40, 41]). Below we will use the value $a_{\mu}^{\text{QED}} = 116584718.08(15) \cdot 10^{-11}$ [42, 43], where the error is dominated by the estimate of the unknown five-loop contributions (for a detailed discussion and more references see e.g. the recent review [44]). The EW corrections are known to two-loop accuracy [45, 46, 47, 48, 49] and amount to $a_{\mu}^{\text{EW}} = (154 \pm 2) \cdot 10^{-11}$, where the error estimate is due to the remaining hadronic uncertainties, the unknown Higgs mass and undetermined higher-order contributions. Clearly, compared with the uncertainties of the VP contributions discussed above, both the QED and EW corrections are very well under control. In the hadronic sector, as well as the (LO and HO) VP corrections, we also have to take into account the light-by-light scattering contributions. They enter at the same order α^3 as the HO VP corrections, but can not be determined from data via dispersive methods. All model-based estimates include the pseudoscalar contributions, i.e. exchanges of π^0 , η and η' , which are leading in the large N_c limit. In addition, axial vector exchanges, charged π and K loops, and (dressed) quark loop diagrams are taken into account, and short-distance constraints from pQCD have been applied to enforce a consistent matching at higher virtualities. Although there are important differences in the treatment of the different contributions, the recent results $a_{\mu}^{\text{had, l-by-l}} = (10.5 \pm 2.6) \cdot 10^{-10}$ [50] and $a_{\mu}^{\text{had, l-by-l}} = (11.6 \pm 4.0) \cdot 10^{-10}$ [51, 44] turn out to be compatible (see also [52] for a recent short review). Note that the recent results from [50] and [51] agree fairly well w.r.t. the leading contributions, and that both have cancellations in the subleading parts, thus strengthening our confidence in the reliability of these

estimates. Also note that these predictions of $a_\mu^{\text{had, l-by-l}}$ are below the estimated upper bound $a_\mu^{\text{had, l-by-l}} < 15.9 \cdot 10^{-10}$ based on parton hadron duality [53]. For our prediction of a_μ^{SM} we will use the result from [50], which has been obtained as a ‘best estimate’ for $a_\mu^{\text{had, l-by-l}}$ after reviewing different approaches. In the future it may well be possible to obtain independent constraints on, or hopefully even a full prediction of, the light-by-light contributions from lattice gauge field theory. Such first principles simulations of the required four-current correlator are very difficult, but work by two groups is underway [54, 55] and the first steps are encouraging.¹⁷ In addition, measurements of the meson form factors, which are needed in the modelling of the light-by-light contributions, may become feasible at several experiments at low energy e^+e^- colliders.

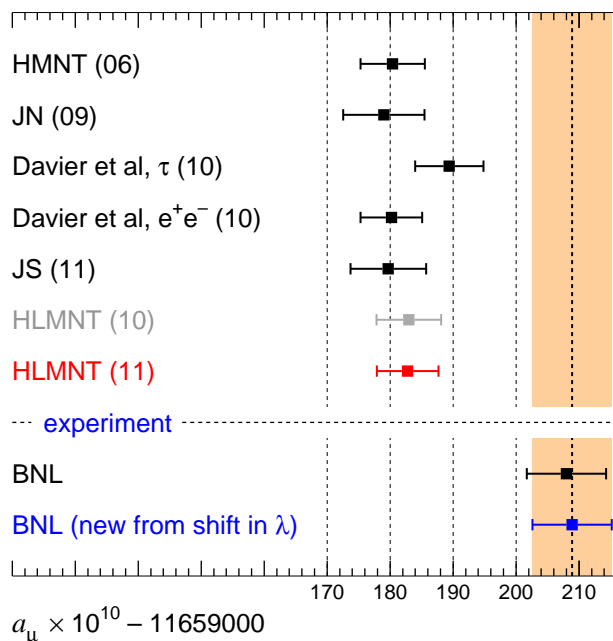


Figure 16: Standard model predictions of a_μ by several groups compared to the measurement from BNL [1, 59, 60]. The SM predictions are from HMNT (06) [6], JN (09) [44], Davier *et al.* [10], JS (11) [18], HLMNT (10) [61], and HLMNT (11) is this work. Note that the value from Jegerlehner and Szafron includes τ spectral function data, which, in their approach, are fully consistent with and confirm the e^+e^- data. HLMNT (10) is a preliminary version of this work, presented at conferences [61], but before the full updated data set was available.

Adding all the hadronic, QED and EW contributions, we finally arrive at the SM prediction

$$a_\mu^{\text{SM}} = (11\,659\,182.8 \pm 4.9) \cdot 10^{-10}, \quad (10)$$

where the errors have been added in quadrature. This prediction is now even slightly more precise than the seminal experimental measurement from BNL [1]. After taking into account

¹⁷For first results obtained within an alternative approach based on Dyson-Schwinger methods see Goecke *et al.* [56]. They estimate $a_\mu^{\text{had, l-by-l}}$ to be largely enhanced by quark loop contributions. However, see [57] for a counter-argument.

the small shift in CODATA’s published ratio of the muon-to-proton magnetic moment [58], the experimental value for a_μ reads [59, 60]

$$a_\mu^{\text{EXP}} = 116\,592\,089(63) \cdot 10^{-11}. \quad (11)$$

This leads to the difference

$$a_\mu^{\text{EXP}} - a_\mu^{\text{SM}} = (26.1 \pm 8.0) \cdot 10^{-10} \quad (12)$$

which corresponds to 3.3σ discrepancy. In Fig. 16 we compare the SM predictions of different groups (markers as indicated) and the BNL measurement, which is displayed by the (orange) band. Note that, despite many changes in the recent history, the different predictions agree very well with each other, and the discrepancy seen in this observable is persisting. While, at a level of 3σ , one can not speak of a firmly established deviation from the SM prediction, all different contributions have been checked thoroughly. It should also be noted that it seems increasingly difficult to explain the discrepancy by a change in the hadronic data alone, as this would lead to increased tension with the EW precision fits of the SM and the current Higgs mass limits [62, 63].

4 $\Delta\alpha(M_Z^2)$

Leptonic and hadronic vacuum polarisation effects screen the electric charge and lead to the scale dependence (‘running’) of the QED coupling, $\alpha(q^2) = \alpha/(1 - \Delta\alpha_{\text{lep}}(q^2) - \Delta\alpha_{\text{had}}(q^2))$, where α is the fine structure constant and $\Delta\alpha(q^2)$ the real part of the vacuum polarisation of the photon. Of particular importance is the value at the scale of the mass of the Z boson, $\alpha(M_Z^2)$. Remarkably, as a consequence of the hadronic uncertainties, this is the least well known of the EW SM parameters, $[G_\mu, M_Z, \alpha(M_Z^2)]$. It is needed for precise predictions of high-energy processes and is a crucial ingredient in the EW precision fits of the SM, which in turn lead to the indirect determination of the Higgs mass.

We can use the same compilation of hadronic data (combined with pQCD) to calculate, with the best possible precision, the hadronic contributions to the running of the QED coupling from the dispersion integral

$$\Delta\alpha_{\text{had}}(q^2) = -\frac{\alpha q^2}{3\pi} P \int_{s_{\text{th}}}^{\infty} \frac{R_{\text{had}}(s') ds'}{s'(s' - q^2)}, \quad (13)$$

where P denotes the principal value of the integral. Above 11.09 GeV we use pQCD to calculate R_{had} . As usual, the contribution from the top quark is added separately. Our new result for the five-flavour hadronic contributions then reads

$$\Delta\alpha_{\text{had}}^{(5)}(M_Z^2) = (276.26 \pm 1.16_{\text{exp}} \pm 0.74_{\text{rad}}) \cdot 10^{-4}. \quad (14)$$

Together with the well known analytic results for the leptonic and the top quark contributions, $\Delta\alpha_{\text{lep}}(M_Z^2) = 0.031498$ [64] and $\Delta\alpha_{\text{top}}(M_Z^2) = -0.0000728(14)$ [65] (where we have used $m_t = (172.0 \pm 1.6)$ GeV [29]), this allows for the further improved prediction

$$\alpha(M_Z^2)^{-1} = 128.944 \pm 0.019. \quad (15)$$

Group, year, ref.	$\Delta\alpha_{\text{had}}^{(5)}(M_Z^2)$	Remarks
Kühn+Steinhauser (98) [66]	0.02775 ± 0.00017	pQCD
Martin <i>et al.</i> (00) [27]	0.02738 ± 0.00020	data driven
Troconiz+Yndurain (05) [67]	0.02749 ± 0.00012	pQCD
Burkhardt+Pietrzyk (05) [68]	0.02758 ± 0.00035	data driven
HMNT (06) [6]	0.02768 ± 0.00022	data driven
Jegerlehner (08) [69]	0.027594 ± 0.000219	data driven/pQCD
	0.027515 ± 0.000149	Adler function ($\sqrt{s_0} = 2.5$ GeV)
Jegerlehner (10) [70]	0.027498 ± 0.000135	Adler function ($\sqrt{s_0} = 2.5$ GeV)
Davier <i>et al.</i> (10) [10]	0.02742 ± 0.00010	pQCD from $1.8 < \sqrt{s} < 3.7$ GeV and for $\sqrt{s} > 5$ GeV
HLMNT (11), this work	0.027626 ± 0.000138	data driven

Table 6: Results for $\Delta\alpha_{\text{had}}^{(5)}(M_Z^2)$ from different groups. The column ‘remarks’ indicates if the analysis is mainly relying on data as input in the dispersion integral (13) or if pQCD is used outside the resonance regions; another approach proposed by Jegerlehner is based on the use of the Adler D function, thus reducing the dependence on data and improving the error.

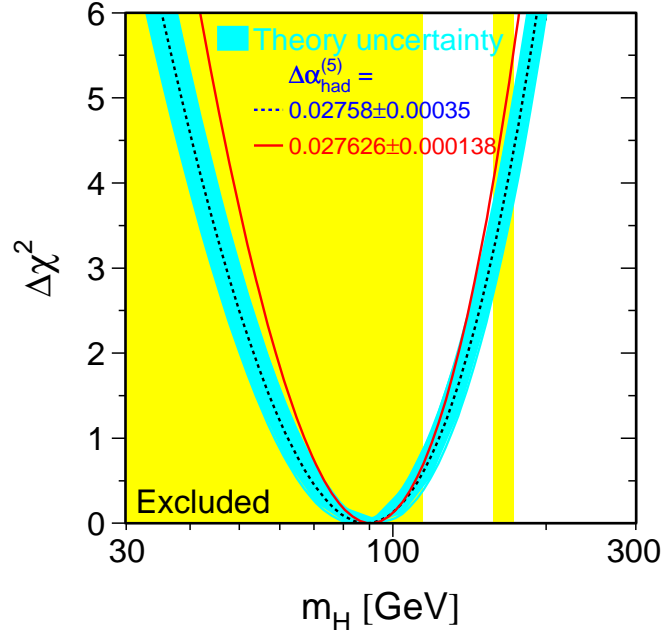


Figure 17: ‘Blue-band plot’ from the LEP EWWG: The dark (blue) band with the dashed line shows the default EW precision data fit result (July 2010), whereas the solid (red) parabola is obtained by using our new value for $\Delta\alpha_{\text{had}}^{(5)}(M_Z^2)$ [72].

In Table 6 we compare our result for $\Delta\alpha_{\text{had}}^{(5)}(M_Z^2)$ with recent evaluations from other groups. Note that our result is slightly bigger and significantly more accurate than the prediction [68] used as default by the LEP Electroweak Working Group for their precision fits [71]. In the so-

called ‘blue-band plot’, which summarises the indirect determination of the Higgs mass, using our new value for $\alpha(M_Z^2)$ results in a steeper parabola, see the solid (red) line in Fig. 17. The fit result for the Higgs mass is $m_H = (91^{+30}_{-23})$ GeV [72], which is to be compared to $m_H = (89^{+35}_{-26})$ GeV for the default fit (July 2010). Together with the regions excluded by direct Higgs searches at LEP and Tevatron (indicated by the shaded (yellow) areas in Fig. 17), this could hint at another problem for the SM, similar to, but less significant than the discrepancy in $g - 2$.

We have also written an easy-to-use Fortran package¹⁸ for the running coupling at space- and time-like momenta, which will be discussed in a separate work [73] (see also chapter 6 in [7] for a recent review). Note that for the analyses of $g - 2$ and $\Delta\alpha$ presented here we have used, for consistency, our own routine for corrections of the data w.r.t. VP effects.

5 Conclusions and Outlook

Here we have been concerned with obtaining the best possible accuracy for the theoretical predictions for the anomalous magnetic moment of the muon, $(g - 2)/2$, and for the QED coupling at the Z -boson mass, $\alpha(M_Z^2)$; two quantities which play a very important role in electroweak precision physics. Indeed, the discrepancy between the SM prediction and the experimental measurement of $g - 2$ is arguably the best hint, at present, of physics beyond the SM. At the moment, the accuracy of the predictions are limited by the uncertainty of the hadronic vacuum-polarisation contributions. We have used all the available data on $e^+e^- \rightarrow$ hadrons to achieve a data-driven determination of these contributions, as accurately as possible. We employ a detailed cluster algorithm, with local χ^2 inflation when necessary, to combine data from different experiments in a reliable and consistent way. From the pie diagrams in the first row of Fig. 18 we see that the dominant contribution to the LO hadronic vacuum-polarisation correction, $a_\mu^{\text{had,LO VP}}$, to $g - 2$ comes from the e^+e^- energy region up to 0.9 GeV, whereas the major part of the error comes from the region up to 2 GeV.

Recently new data for many exclusive channels in the low to intermediate energy region have become available, both from direct scan experiments and from analyses of radiative return measurements. In the 2π channel, the different experiments show slight disagreement. In particular, there is tension between the radiative return results obtained from the KLOE and BaBar experiments, with the BaBar data significantly higher than the KLOE data especially at larger energies. The tension prevents a bigger improvement of the error on the contribution from this important region than might have been expected, given the increased statistics; but it also means that there clearly is still scope for improved accuracy from future measurements.

There is the possibility of evaluating the contribution in the e^+e^- energy region 1.43–2 GeV, *either* by using the data for the inclusive $e^+e^- \rightarrow$ hadrons cross section, *or* by using the sum of the cross sections for all the exclusive e^+e^- cross sections. There is a discrepancy between the two alternatives, and, in the past, we had used a sum-rule analysis [2] to distinguish between them. However, in the region below 2 GeV, many exclusive channels with higher multiplicities are now much better probed through the radiative return analyses of the BaBar data, and the

¹⁸The whole package is available upon request from the authors as a self-contained collection of Fortran routines and includes the real and imaginary part of the leptonic and hadronic vacuum polarisation.

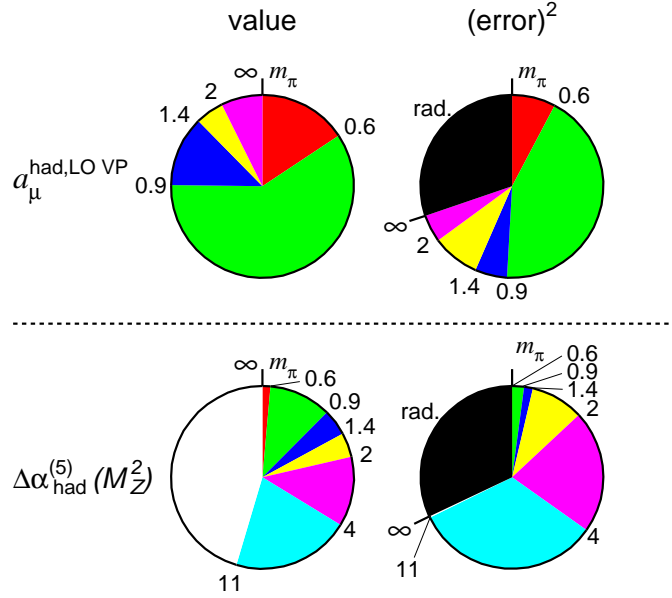


Figure 18: The pie diagrams in the left- and right-hand columns show the fractions of the total contributions and $(\text{errors})^2$, respectively, coming from various energy intervals in the dispersion integrals (2) and (13). The pie diagrams for the LO hadronic contribution to $g - 2$, shown in the first row, correspond to sub-contributions with energy boundaries at $m_\pi, 0.6, 0.9, 1.4, 2$ GeV and ∞ , whereas for the hadronic contribution to the QED coupling, shown in the second row, the boundaries are at $m_\pi, 0.6, 0.9, 1.4, 2, 4, 11.09$ GeV and ∞ . In the $(\text{error})^2$ pie diagrams we also included the $(\text{error})^2$ arising from the treatment of the radiative corrections to the data.

sum of the exclusive channels is better determined. This has prompted us to re-investigate the sum-rule analysis including the new data in the input. We now find good agreement of the sum-rules with the world average value of α_s if the sum of exclusive channels is used, which is slightly higher than the inclusive data, and a worsened agreement if inclusive data are input. We therefore now use the exclusive data, which are also more accurate.

Furthermore, new much more accurate BES data are seen to be in perfect agreement with the pQCD predictions of $e^+e^- \rightarrow \text{hadrons}$ in the range from 2.6 GeV up to the charm threshold. We therefore use pQCD in this region, but with a conservative error of about 3.5% corresponding to the accuracy of the latest BES data. Use of pQCD from 2 GeV would result in a slight shift ($-1.2 \cdot 10^{-10}$ for a_μ), with an even stronger preference for the exclusive data in the sum-rule analysis, see Fig. 12.

In summary, we find the updated LO and HO hadronic vacuum-polarisation corrections to be

$$a_\mu^{\text{had, LO VP}} = (694.91 \pm 4.27) \cdot 10^{-10}, \quad (16)$$

$$a_\mu^{\text{had, HO VP}} = (-9.84 \pm 0.07) \cdot 10^{-10}. \quad (17)$$

When the representative value of the hadronic light-by-light correction,

$$a_{\mu}^{\text{had,l-by-l}} = (10.5 \pm 2.6) \cdot 10^{-10}, \quad (18)$$

and the QED and EW contributions are added, our SM prediction for the anomalous magnetic moment of the muon is

$$a_{\mu}^{\text{SM}} = (11\,659\,182.8 \pm 4.9) \cdot 10^{-10}, \quad (19)$$

which is a slight shift and improvement of our earlier result [6], $a_{\mu}^{\text{SM}}(\text{HMNT } 06) = (11\,659\,180.4 \pm 5.1) \cdot 10^{-10}$. More important, despite many changes in the data, the SM prediction of $g - 2$ is further consolidated, and with it the discrepancy of 3.3σ between the BNL measurement and the SM prediction. Moreover, there is also agreement with other independent analyses, which use somewhat different treatments of the data.

There is great potential for further improvements in both the experimental and theoretical determinations of $g - 2$ of the muon. On the experimental side, the experiments CMD-3 and SND at VEPP-2000 in Novosibirsk have already started taking data. More radiative return analyses from BaBar and KLOE are in preparation. Also more measurements from BES are anticipated. In the longer term, there are prospects for an upgrade of DAΦNE and for SuperB factories. These experiments will allow a further reduction of the error on the calculation of the hadronic vacuum polarisation contributions, which will be essential in view of the next generation measurements of $g - 2$ planned at Fermilab and at J-PARC. In fact, then the error on the calculation of the hadronic light-by-light contributions will become critical. Indeed, for the theoretical prediction to continue to match the experimental measurement of $g - 2$ in precision, it is clear that theoretical efforts, together with measurements of the two-photon form factors of scalars and pseudo-scalars, are needed to improve the model predictions in the light-by-light sector. The $g - 2$ discrepancy has implications for constraining SUSY models as we discussed in [2]; for a very recent application and further references see [74].

As a by-product of the $g - 2$ analysis, we used the same compilation of hadronic data to update the prediction of the value of the QED coupling, whose value at the Z scale is

$$\alpha(M_Z^2)^{-1} = 128.944 \pm 0.019. \quad (20)$$

In this case, we see from Fig. 18 that the contributions to $\Delta\alpha_{\text{had}}^{(5)}(M_Z^2) = (276.26 \pm 1.38) \cdot 10^{-4}$ have quite a different dependence on the e^+e^- energy, with much less reliance on the lower energies. When this value for $\Delta\alpha_{\text{had}}^{(5)}(M_Z^2)$ is used in the EW precision fits of the SM, the Higgs mass is constrained more tightly, with its optimum value in a region excluded by the direct searches, namely $m_H = (91^{+30}_{-23})$ GeV at 68% confidence level.

Acknowledgments

We thank Martin Grünewald for providing us with the ‘blue-band plot’ using our value of $\Delta\alpha_{\text{had}}^{(5)}(M_Z^2)$. We also thank M. Davier, S. Eidelman, A. Hoecker, F. Jegerlehner, B. Malaescu and G. Venanzoni for valuable discussions.

References

- [1] G. W. Bennett *et al.*, Phys. Rev. **D73** (2006) 072003.
- [2] K. Hagiwara, A. D. Martin, Daisuke Nomura and T. Teubner, Phys. Rev. **D69** (2004) 093003; Phys. Lett. **B557** (2003) 69.
- [3] KLOE Collaboration, F. Ambrosino *et al.*, Phys. Lett. **B670** (2009) 285.
- [4] KLOE Collaboration, F. Ambrosino *et al.*, Phys. Lett. **B700** (2011) 102.
- [5] BaBar Collaboration, B. Aubert *et al.*, Phys. Rev. Lett. **103** (2009) 231801.
- [6] K. Hagiwara, A. D. Martin, Daisuke Nomura and T. Teubner, Phys. Lett. **B649** (2007) 173.
- [7] S. Actis *et al.*, Eur. Phys. J. **C66** (2010) 585, [arXiv:0912.0749](#).
- [8] F. Ignatov (for the CMD-2 and SND Collaborations), Nucl. Phys. Proc. Suppl. **181-182** (2008) 101.
- [9] KLOE Collaboration, A. Aloisio *et al.*, Phys. Lett. **B606** (2005) 12.
- [10] M. Davier, A. Hoecker, B. Malaescu and Z. Zhang, Eur. Phys. J. **C71** (2011) 1515, [arXiv:1010.4180 \[hep-ph\]](#).
- [11] CMD-2 Collaboration, R. R. Akhmetshin *et al.*, Phys. Lett. **B578** (2004) 285, [arXiv:hep-ex/0308008](#).
- [12] CMD-2 Collaboration, R. R. Akhmetshin *et al.*, Phys. Lett. **B648** (2007) 28, [arXiv:hep-ex/0610021](#).
- [13] SND Collaboration, M. N. Achasov *et al.*, J. Exp. Theor. Phys. **103** (2006) 380 [Zh. Eksp. Teor. Fiz. **130** (2006) 437], [arXiv:hep-ex/0605013](#).
- [14] M. Davier, A. Hoecker, B. Malaescu, C. Z. Yuan and Z. Zhang, Eur. Phys. J. **C66** (2010) 1.
- [15] C. E. Wolfe and K. Maltman, Phys. Rev. **D83** (2011) 077301, [arXiv:1011.4511](#).
- [16] M. Davier *et al.*, Eur. Phys. J. **C66** (2010) 127, [arXiv:0906.5443 \[hep-ph\]](#).
- [17] M. Benayoun, P. David, L. DelBuono and O. Leitner, Eur. Phys. J. **C65** (2010) 211, [arXiv:0907.4047 \[hep-ph\]](#); Eur. Phys. J. **C68** (2010) 355, [arXiv:0907.5603 \[hep-ph\]](#); see also Chinese Phys. **C34** (2010) 698, [arXiv:0912.1248 \[hep-ph\]](#).
- [18] F. Jegerlehner and R. Szafron, Eur. Phys. J. **C71** (2011) 1632, [arXiv:1101.2872 \[hep-ph\]](#).
- [19] I. B. Logashenko (on behalf of the CMD-3 and SND collaborations), Chinese Phys. **C34** (2010) 669.
- [20] BaBar Collaboration, B. Aubert *et al.*, Phys. Rev. **D71** (2005) 052001.
- [21] BaBar Collaboration, B. Aubert *et al.*, Phys. Rev. **D77** (2008) 092002.
- [22] BaBar Collaboration, B. Aubert *et al.*, Phys. Rev. **D76** (2007) 092005.

- [23] BaBar Collaboration, B. Aubert *et al.*, Phys. Rev. **D73** (2006) 052003.
- [24] K. Hagiwara, R. Liao, A. D. Martin, Daisuke Nomura and T. Teubner, Chinese Phys. **C34** (2010) 728, [arXiv:1001.5401 \[hep-ph\]](#).
- [25] A. Cordier *et al.*, Phys. Lett. **106B** (1981) 155.
- [26] BaBar Collaboration, J. P. Lees *et al.*, [arXiv:1103.3001 \[hep-ex\]](#).
- [27] A. D. Martin, J. Outhwaite and M. G. Ryskin, Phys. Lett. **B492** (2000) 69.
- [28] P. A. Baikov, K. G. Chetyrkin and J. H. Kühn, Phys. Rev. Lett. **101** (2008) 012002, [arXiv:0801.1821 \[hep-ph\]](#).
- [29] K. Nakamura *et al.* (Particle Data Group), J. Phys. **G37** (2010) 075021.
- [30] CMD-2 Collaboration, R. R. Akhmetshin *et al.*, Phys. Lett. **B669** (2008) 217.
- [31] SND Collaboration, M. N. Achasov *et al.*, Phys. Rev. **D76** (2007) 072012.
- [32] SND Collaboration, M. N. Achasov *et al.*, J. Exp. Theor. Phys. **103** (2006) 720.
- [33] CMD-2 Collaboration, R. R. Akhmetshin *et al.*, Phys. Lett. **B642** (2007) 203.
- [34] KLOE Collaboration, F. Ambrosino *et al.*, Phys. Lett. **B669** (2008) 223.
- [35] BES Collaboration, M. Ablikim *et al.*, Phys. Rev. Lett. **97** (2006) 262001.
- [36] BES Collaboration, M. Ablikim *et al.*, Phys. Lett. **B677** (2009) 239.
- [37] CLEO Collaboration, D. Besson *et al.*, Phys. Rev. **D76** (2007) 072008.
- [38] R. V. Harlander and M. Steinhauser, Comput. Phys. Commun. **153** (2003) 244, [arXiv:hep-ph/0212294](#).
- [39] T. Aoyama, M. Hayakawa, T. Kinoshita and M. Nio, Phys. Rev. **D78** (2008) 113006, [arXiv:0810.5208 \[hep-ph\]](#).
- [40] K. Asano, M. Hayakawa, T. Kinoshita, M. Nio and N. Watanabe, Phys. Rev. **D81** (2010) 053009, [arXiv:1001.3704 \[hep-ph\]](#).
- [41] T. Aoyama, M. Hayakawa, T. Kinoshita and M. Nio, Phys. Rev. **D82** (2010) 113004, **D83** (2011) 053002, **D83** (2011) 053003.
- [42] T. Kinoshita and M. Nio, Phys. Rev. **D73** (2006) 053007.
- [43] T. Aoyama, M. Hayakawa, T. Kinoshita and M. Nio, Phys. Rev. **D77** (2008) 053012.
- [44] F. Jegerlehner and A. Nyffeler, Phys. Rept. **477** (2009) 1, [arXiv:0902.3360 \[hep-ph\]](#).
- [45] A. Czarnecki, W. J. Marciano and A. Vainshtein, Phys. Rev. **D67** (2003) 073006, Erratum-ibid. **D73** (2006) 119901, [arXiv:hep-ph/0212229](#).
- [46] A. Czarnecki, B. Krause and W. J. Marciano, Phys. Rev. Lett. **76** (1996) 3267, [arXiv:hep-ph/9512369](#).
- [47] A. Czarnecki, B. Krause and W. J. Marciano, Phys. Rev. **D52** (1995) 2619, [arXiv:hep-ph/9506256](#).

- [48] M. Knecht, S. Peris, M. Perrottet and E. De Rafael, JHEP **0211** (2002) 003, [arXiv:hep-ph/0205102](#).
- [49] S. Peris, M. Perrottet and E. de Rafael, Phys. Lett. **B355** (1995) 523, [arXiv:hep-ph/9505405](#).
- [50] J. Prades, E. de Rafael and A. Vainshtein, [arXiv:0901.0306 \[hep-ph\]](#).
- [51] A. Nyffeler, Phys. Rev. **D79** (2009) 073012, [arXiv:0901.1172 \[hep-ph\]](#).
- [52] A. Nyffeler, Chinese Phys. **C34** (2010) 705, [arXiv:1001.3970 \[hep-ph\]](#).
- [53] J. Erler and G. T. Sanchez, Phys. Rev. Lett. **97** (2006) 161801, [arXiv:hep-ph/0605052](#).
- [54] T. Blum and S. Chowdhury, Nucl. Phys. Proc. Suppl. **189** (2009) 251; S. Chowdhury *et al.*, PoS LATTICE2008 (2008) 251.
- [55] P. Rakow, *private communications*; see also talk at *Lattice 2008*, Williamsburg, Virginia, USA, 14–19 July 2008, http://conferences.jlab.org/lattice2008/talks/parallel/paul_rakow.pdf.
- [56] T. Goecke, C. S. Fischer and R. Williams, Phys. Rev. **D83** (2011) 094006, [arXiv:1012.3886](#).
- [57] R. Boughezal and K. Melnikov, [arXiv:1104.4510 \[hep-ph\]](#).
- [58] P. J. Mohr, B. N. Taylor and D. B. Newell (CODATA 2006), Rev. Mod. Phys. **80** (2008) 633, [arXiv:0801.0028 \[physics.atom-ph\]](#).
- [59] B. L. Roberts, Chinese Phys. **C34** (2010) 741, [arXiv:1001.2898 \[hep-ex\]](#).
- [60] C. Amsler *et al.* (Particle Data Group), Phys. Lett. **B667** (2008) 1.
- [61] K. Hagiwara, R. Liao, A. D. Martin, Daisuke Nomura and T. Teubner, AIP Conf. Proc. **1343** (2011) 340; in the proceedings of *Tau2010, 11th International Workshop on Tau Lepton Physics, Manchester, U.K., 13–17 September 2010*, to appear in Nucl. Phys. **B** (Proc. Suppl.).
- [62] M. Passera, W. J. Marciano and A. Sirlin, Phys. Rev. **D78** (2008) 013009, [arXiv:0804.1142 \[hep-ph\]](#).
- [63] M. Passera, W. J. Marciano and A. Sirlin, Chinese Phys. **C34** (2010) 735, [arXiv:1001.4528 \[hep-ph\]](#).
- [64] M. Steinhauser, Phys. Lett. **B429** (1998) 158.
- [65] K. G. Chetyrkin, J. H. Kühn and M. Steinhauser, Phys. Lett. **B371** (1996) 93; Nucl. Phys. **B482** (1996) 213; Nucl. Phys. **B505** (1997) 40.
- [66] J. H. Kühn and M. Steinhauser, Phys. Lett. **B437** (1998) 425, [arXiv:hep-ph/9802241](#).
- [67] J. F. de Troconiz and F. J. Yndurain, Phys. Rev. **D71** (2005) 073008, [arXiv:hep-ph/0402285](#).
- [68] H. Burkhardt and B. Pietrzyk, Phys. Rev. **D72** (2005) 057501, [arXiv:hep-ph/0506323](#).

- [69] F. Jegerlehner, Nucl. Phys. Proc. Suppl. **181-182** (2008) 135, [arXiv:0807.4206 \[hep-ph\]](#).
- [70] F. Jegerlehner, talk presented at the *LC10 Workshop, INFN/LNF Frascati, Italy, December 2010*, [arXiv:1107.4683 \[hep-ph\]](#).
- [71] For latest results of the ‘LEP Electroweak Working Group’ (LEP EWWG) see <http://lepewwg.web.cern.ch/LEPEWWG/>.
- [72] M. Grünewald, *private communications*. For a description of the procedure used see: ALEPH Collaboration, [arXiv:1012.2367 \[hep-ex\]](#).
- [73] K. Hagiwara, R. Liao, A. D. Martin, Daisuke Nomura and T. Teubner, in preparation.
- [74] G. C. Cho, K. Hagiwara, Y. Matsumoto and D. Nomura, [arXiv:1104.1769](#).